Carotid Atherosclerosis Assessment with 3D Ultrasound

A Review of the Master's Thesis

José Carlos Rosa Seabra

1 Introduction

In most western countries, atherosclerosis is the most prevalent and main cause of death, representing more than twice the number of deaths due to cancer and 10-fold the deaths caused by accidents. It is a disease of the large and medium size arteries and its most important feature is plaque formation due to sub-endothelial accumulation of lipid, protein, and cholesterol esters [1].

The risk of stroke increases with the severity of carotid stenosis and decreases after endarterectomy, i.e. surgical removal of plaque [2]. Up to now the degree of stenosis has been targeted as one of the most important landmarks to assess the risk of stroke [3]. Indeed, it is the only criterion currently used to decide about a surgical intervention. Other factors, however, also start to be used, such as, cross-sectional area of stenosis, surface morphology, composition [4] and texture [5].

Large clinical trials (NASCET, ECST, ACST, ACAS)[6] performed in both symptomatic and asymptomatic patients, were able to identify groups that clearly benefit with the surgery. Moreover, it is known that is necessary to operate 83 asymptomatic patients, with more than 60% stenosis, to prevent one stroke, which means that there is still a large number of individuals to whom the clinical decision remains uncertain and may not benefit from surgery. The decision on whether or not to operate is clinically relevant and has financial consequences and therefore accurate diagnostic tools are needed.

In order to increase the accuracy of the diagnosis, parameters aiming to identify vulnerable lesions have been studied using 2D B-mode ultrasound (US) imaging with computer-assisted analysis [7]. US images are used, for instance, to extract the carotid contours to measure the stenosis severity [8,9], to automatically or semi-automatically segment the intima-media layer thickness (IMT) [10] and to segment and characterize the plaques with respect to their instability , based on intensity and texture [11,12]. However, 2D assessment of plaque echoic features may not be very accurate because it depends on the selection of a representative ultrasound image of the plaque. For this reason, an

increasing amount of work has been published proposing new methods based on 3D ultrasound, where 3D reconstructions are used to better assess plaque vulnerability.

3D ultrasound uses a sequence of ultrasound images corresponding to different positions and orientations of the ultrasound probe. Based on this information, it is possible to compute the spatial position of every pixel from every image to estimate a given 3D region of interest (ROI) [13], which describes the carotid and plaque anatomies. The probe can be manipulated by using mechanical devices or directly by the medical doctor in a freehand basis. Usually, in both cases, a spatial locator is attached to the ultrasound probe to measure its position. However, these devices are expensive and are not usually provided with the traditional ultrasound equipment. Hence, 3D ultrasound algorithms require specialized experimental setup which is only available in academic laboratories or highly technological equipped medical centers.

In this work, it is proposed a rigid acquisition protocol and a reconstruction algorithm that does not need any device for spatial location to obtain the volume reconstruction. The anatomy and location of the carotid makes it possible to keep a uniform sweep velocity of the ultrasound probe while a set of nearly orthogonal cross sections are acquired. The program that implements the reconstruction algorithm uses either the feature-based reconstruction, to obtain realistic carotid and plaque 3D models, and the voxel-based approach, for the plaque characterization. The program also includes a semi-automatic method for plaque characterization, based on global morphology and textural properties in three-dimensions, presenting a user-friendly interface for the visualization of the results. A novel local analysis approach is also introduced, regarding the identification of vulnerable and potentially dangerous locations within the plaque.

2 Problem Formulation

The common carotid is the major artery which supplies the brain, and face and neck tissues with blood. It is located in the lateral side of the neck, along its longitudinal axis. This artery branches off in the external and internal carotids, behind the mandibular angle, along the upward direction (see fig.1).

The most frequent location of the atherosclerotic lesion in the cerebro-vascular sector is in the common carotid bifurcation (see fig.1) and in the origin of the internal carotid artery (carotid bulb) where plaque formation tends to produce obstruction or stenosis, reducing the blood flow, or to cause liberation of thrombi or plaque fragments that embolize further ahead.

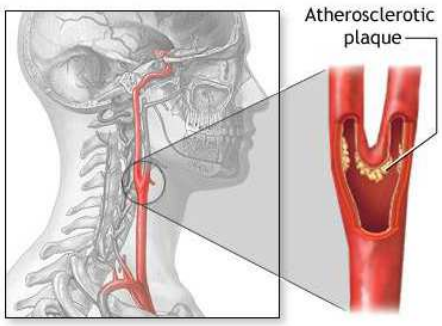

Figure 1. Carotid artery anatomy and location. Atherosclerotic plaque-prone regions.

The first step of this project is to acquire parallel cross sections of the carotid to build a 3D mesh representing its anatomy. Since no spatial locators are being used, the acquisition protocol is a critical process to guarantee the quality of the results. The ultrasound probe must be manipulated as uniformly as possible from the base of the neck up to the base of the skull, keeping its orientation as static as possible.

All ultrasound exams were performed on a Philips HDI 5000 duplex scanner (Philips Medical Ultrasound, NL) with a 5 to 12 MHz dynamic range linear transducer, operating on *Brightness Mode*. In a typical acquisition session 60 images are acquired during a period of 2 seconds. The ultrasound image sequences in AVI format are then stored on optical disc.

Small variations on the orientation of the ultrasound probe are not critical because the algorithm performs the alignment of the images. The acquisition protocol is illustrated in fig. 2, where the metallic strips, separated by a known distance, are used as landmarks for signaling the limits of the ultrasound probe course.

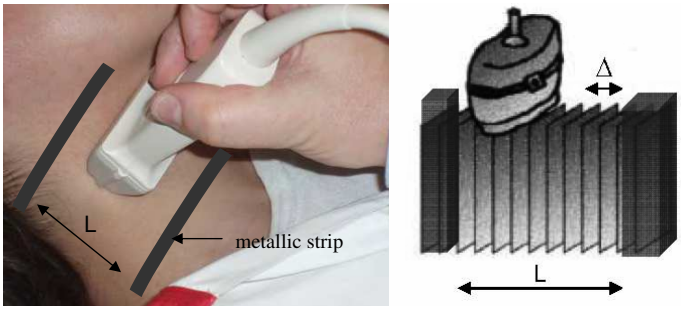

Figure 2. Acquisition protocol. The US probe is placed transversally to the neck and the image sequence is recorded by sweeping the probe over a known course.

Small variations on the sweep velocity, $V = V_0 + \Delta_V$ with $\Delta_V < 0.1V_0$ and $V_0 = 8cm/2sec = 4cm/sec$, leads to position errors $\leq 0.02cm$, which are small

when compared with the total length of the probe course, $d = 8cm$.

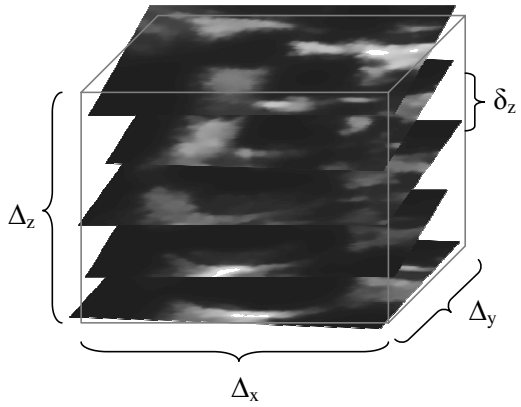

Figure 3. Sequence of cross-sections used for 3D ultrasound (Dimensions of the region of interest are also indicated).

The reconstruction of carotid and plaque borders is obtained from a set of N images, approximately parallels and separated by

$$\delta_z = \Delta_z/(N-1) \tag{1}$$

where Δ_z is the total length of the probe course (see fig. 3), delimited by the strips. The position of each pixel is computed as

$$x^p_{i,j} = (i\delta_x, j\delta_y, p\delta_z) \tag{2}$$

where p is the index of the image, δ_x and δ_y are the inter-pixel distances which are constant for all images and given by the ultrasound equipment and δ_z is obtained from (1).

3 Reconstruction

The reconstruction of the carotid and plaque is performed using a feature-based approach where the contours of both structures are extracted from each image of the data sequence. To produce the final meshes these contours are linked, regularized, aligned and longitudinally smoothed.

Since the spatial information inside the lesion is clinically relevant, voxel-based reconstruction is also performed, only inside the plaques, to allow the assessment of its global and local instability.

The reconstruction is performed offline with a program written in-house, implemented in Matlab (Mathworks, Inc.). This program is available, for free

use, in [14], as well as the plaque characterization program and its interface.

3.1 Pre-processing

The ultrasound images usually present a small signal to noise ratio and are corrupted by a type of multiplicative noise called *speckle*, that appears in processes involving coherent radiation like Laser [15], SAR [16] and ultrasound [17]. In this case, the noise is particularly severe.

Bayesian methods have been also successfully used in several medical imaging modalities [18,19]. However, these algorithms are time consuming and computationally demanding. Here, it is used a fast and computational efficient denoising algorithm, based on the Bayesian algorithm described in [20].

The denoising process uses the *maximum a posteriori* (MAP) criterion, with a *total variation* (TV) edge preserving Gibbs prior. The method is formulated as an optimization task which is solved by using the Lyapunov equation [21]. This equation is very important in the Control theory, namely in the stability analysis, optimal control and stochastic control fields. By this, efficient and fast algorithms have been proposed to solve this equation [22–24], which can be used to implement fast and efficient denoising algorithms.

The MAP solution is obtained as follows,

$$F = \arg\min_{F} \left[\underbrace{E_Y(Y,F) + E_F(F)}_{E(Y,F)} \right] \tag{3}$$

where $E(Y,F)$ is an energy function, $E_Y(Y,F)$ is the so called *data fidelity term*, $E_F(F)$ is the prior term, F is a $N \times M$ dimensional matrix representing the denoised image to be estimated and Y is the $N \times M$ noisy observed image.

By using the MAP criterion the data fidelity term is $E_Y = -\log p(Y|F)$ and the prior term is, in this project, obtained from a Gibbs distribution, which is equivalent to model F as a *Markov random field* (MRF) [25],

$$E_F(F) = \alpha TV(F) \tag{4}$$

where α is a parameter to tune the regularization strength and $TV(F)$ is the *Total Variation (TV)* [26] of the field F, defined as follows,

$$TV(F) = \sum_{i,j} g_{i,j} \tag{5}$$

where $g_{i,j}$ is the gradient magnitude at pixel $f_{i,j}$, which can be approximated by using the first order differences,

$$g_{i,j} = \sqrt{(f_{i,j} - f_{i-1,j})^2 + (f_{i,j} - f_{i,j-1})^2}. \tag{6}$$

Assuming statistical independence of the observations and a Rayleigh distribution,

$$p(y_{i,j}|f_{i,j}) = (y_{i,j}/f_{i,j})e^{-y_{i,j}^2/2f_{i,j}} \tag{7}$$

to model the multiplicative noise that corrupts the ultrasound images the energy function is the following

$$E_Y = -\sum_{i,j}\left[\log\left(\frac{y_{i,j}}{f_{i,j}}\right) - \frac{y_{i,j}^2}{2f_{i,j}}\right]. \tag{8}$$

The minimization of $E(Y, F)$ w.r.t. F is obtained by solving the following set of equations,

$$\frac{\partial E(Y,F)}{\partial f_{i,j}} = \frac{\partial E_Y(Y,F)}{\partial f_{i,j}} + \frac{\partial E_F(F)}{\partial f_{i,j}} = 0 \tag{9}$$

for $0 \leq i \leq N-1$ and $0 \leq j \leq M-1$. The non quadratic energy function (3) can be iteratively minimized by solving a set of quadratic energy functions using a *majorize/minimize (MM)* algorithm [27] as described in [28]. Equations (9) can be rewritten, as shown in [21], in the following matrix format

$$W(F).(F - F^{ML}) + 2\alpha(AF + FB) = 0 \tag{10}$$

where "." denotes the Hadamard product, $[F^{ML}]_{i,j} = y_{ij}^2/2$ is the *maximum likelihood (ML) estimate* and $[W]_{i,j} = g_{i,j}/f_{i,j}^2$. $A = \theta_v^T\theta_v$ and $B = \theta_h^T\theta_h$, where θ_v and θ_h are $N \times N$ and $M \times M$difference operators respectively, with the following structure

$$\theta = \begin{pmatrix} 1 & -1 & 0 & ... & 0 & 0 & 0 \\ -1 & 1 & 0 & ... & ... & ... & 0 \\ 0 & -1 & 1 & ... & ... & ... & 0 \\ ... & ... & ... & ... & ... & 1 & 0 \\ 0 & 0 & 0 & ... & ... & -1 & 1 \end{pmatrix}. \tag{11}$$

By using the fixed point method, equation (10) can be solved as follows:

$$\begin{aligned} \mathcal{A}F + F\mathcal{B} + Q_{t-1} &= 0 \\ Q_{t-1} = W_{t-1}.(F_{t-1} - F^{ML}) &- F_{t-1} \end{aligned} \tag{12}$$

where $\mathcal{A} = I_N/2 + 2\alpha A$ and $\mathcal{B} = I_M/2 + 2\alpha B$. I_N and I_M are N and M dimensional square identity matrices respectively, $[W_{t-1}]_{ij} = g_{ij}(t-1)/f_{ij}^2(t-1)$, where $t-1$ denotes the previous iteration. Equation (12) is the well known Sylvester equation which can be solved with fast and efficient algorithms described in the literature [29]. These are implemented at several scientific software packages, such as *Matlab* (Mathworks, Inc.) or *Mathematica* (Wolfram Research, Inc.).

The iterative algorithm defined in (12) can be unstable and the convergence conditions are strongly dependent on the prior parameter α. To overcome this difficulty, a continuation method [30] is used where the $\alpha_t = \alpha_{t-1} - \beta(\alpha_{t-1} - \alpha_d)$ is the parameter at iteration t, β (≈ 0.5) is the decreasing rate and α_d is the final desired value for the parameter, tuned in a trial and error basis.

The processing time is an important constraint in this algorithm because the data sequence contains a large number of images that must be processed in a acceptable time, during the medical exam. Therefore, to reduce the processing time of the overall sequence, the iterative algorithm used to filter each noisy image, described in (12), is initialized with the previously filtered image of the sequence. This procedure is based on the assumption that consecutive images are similar and therefore, the previous filtered image is a good (closed) starting point for the iterative algorithm that is used to filter the current image. Fig. 4 displays an example of pre-processing results of a 346×440 pixel ultrasound noisy image (fig. 4a) using two methods: i) a common despeckling filter [31,32] formed by a combination of a 10×10 window median filter with a $\sigma = 3$ gaussian gilter (fig. 4b) and ii) the MAP despeckling method proposed here (fig. 4c). In this example, it is clear a better performance of the MAP method at the transitions which allows to preserve the anatomic details with clinical relevance.

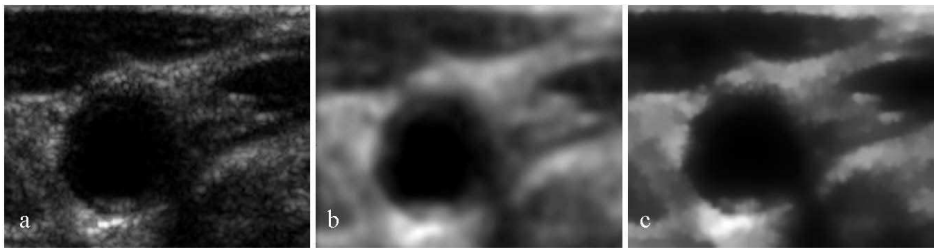

Figure 4. Comparative outcome of different pre-processing methods. a) Original (noisy) ultrasound image, b) denoised image, with median and gaussian filters and c) denoised image, using a MAP criterion and a TV edge preserving prior.

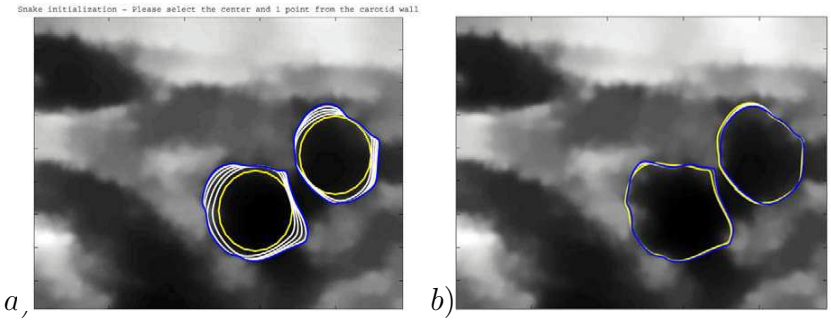

Figure 5. Automatic segmentation. a) Initialization and evolution of the active contours. The resulting contours are used as initial estimations for the second segmentation (b).

3.2 Contour extraction and re-sampling

Next, the process for extracting and re-sampling the contours of the carotid and atheromatous plaque, based on the pre-processed images, is described.

3.2.1 Segmentation

The segmentation is obtained by using an active contours algorithm (usually called snake) described in [33], which is based on the *Gradient Vector Flow* (GVF). The active contour is defined by a set of linked control points, which converges from an initial conformation to a final one, as the result of the application of external forces, depending on the image, and internal forces used to allow consistency in the final result.

In this work, the GVF active contour algorithm is used to automatically segment the anatomic objects present in the image under medical supervision. An exception is made in the first image of the sequence, where the medical doctor must manually define the centers of the carotids and one point from each carotid wall (see fig. 5a). Under regular conditions, the initial contour

used by the GVF algorithm is obtained from the result of the previous segmentation process, as displayed in fig. 5b. However, the medical doctor may interfere with the process, by changing the initial contour or by changing the default parameters used by the GVF algorithm associated with the internal and external energies of the contour.

This functionality is useful when the GVF algorithm wrongly converges due to bad initialization or, more important, when topological modifications arise. Two important situations need a special initialization:

(1) The segmentation of the first image in the bifurcation region, where two contours must be merged into a single one (see fig. 6). Both contours, obtained from the image previous to the bifurcation (fig. 6a) are used to initialize two different contours which intersect, after convergence, in the bifurcation plane (fig. 6b). The new single contour (fig. 6c) results from these two contours by removing the intersection region; finally, the composed contour is used as initialization to segment the carotid in the bifurcation region (fig. 6d). Fig. 6e shows the segmentation result on the bifurcation and on its previous plane.
(2) The segmentation in the first image where a plaque is detected. In this case, the medical doctor must initialize manually the plaque contour. In the next images, the plaque segmentation is made automatically as described above. However, in order to force consistency of both contours, carotid and plaque, a post processing is needed. This procedure consists in the extraction of the plaque region from the intersection between the new contour defined for the plaque and the already existing one for the carotid, as well as, the correction of the carotid artery wall, by removing the region of the plaque.

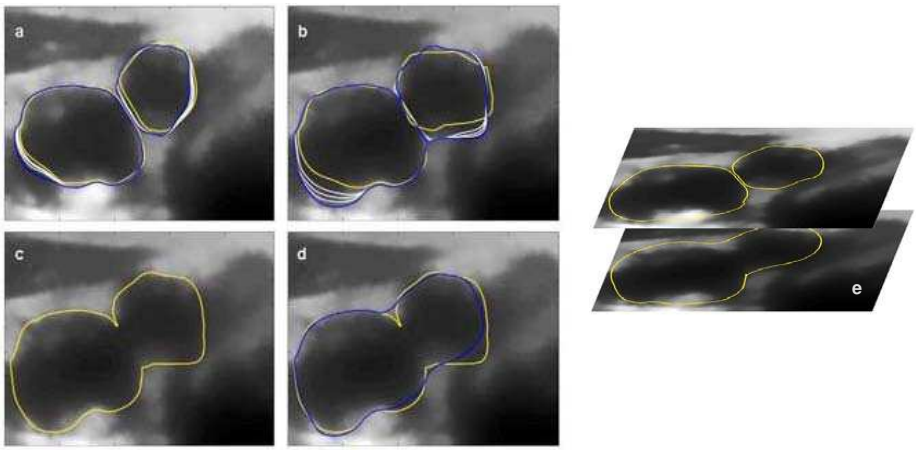

Figure 6. Segmentation of the carotid artery bifurcation.

The final procedure in the segmentation step is the re-sampling and regularization of the contours provided by the GVF algorithm, which are described

by a set of non evenly spaced control points. This non uniform distribution of the control points along the contour makes the correspondence and contours linking an extremely difficult task, however needed to build the 3D mesh from the 2D contours extracted from each image. Therefore, before the linking step, a re-sampling procedure is implemented to change the position of the control points, by distributing them uniformly along the contour. This operation also smoothes the contours according to a regularized parameter controlled by the medical doctor.

3.2.2 Re-sampling

Let $c(s) = [x(s), y(s)]$ be the closed contour to be re-sampled, where $0 \leq s \leq 1$. The control points describing this contour are $p_i = [x_i(s_i), y_i(s_i)]$ where s_i are the normalized positions of each point, along the contour, that is, $s_0 = 0$ and $s_{M-1} = 1$. Here, the M control points are considered noisy observations of the unknown curve $c(s)$ that must be estimated. The contour is described by the following linear combination of N basis functions,

$$x(s) = \sum_{k=0}^{N-1} a_k \phi_k(s) \tag{13}$$

$$y(s) = \sum_{k=0}^{N-1} b_k \phi_k(s) \tag{14}$$

where $\phi_k(s) = sinc(s/\Delta - k)$ are the N basis function used to represent $c(s)$. The goal is to estimate the vectors $A = [a_0, ..., a_{N-1}]^T$ and $B = [b_0, ..., b_{N-1}]^N$ from the observations, i.e., the new control points. Using matrix notation,

$$\hat{x}(s) = \Phi(s)^T A \tag{15}$$

$$\hat{y}(s) = \Phi(s)^T B \tag{16}$$

where $\Phi(s) = [\phi_0, \phi_1, ..., \phi_{N-1}]^T$ is a column vector of the N basis functions computed at position s. The estimation of A (B is estimated in the same way) is performed by minimizing the following energy function,

$$E = (X - \Theta A)^T (X - \Theta A) + \alpha (\theta A)^T (\theta A) \tag{17}$$

where

$$\theta = \begin{pmatrix} 1 & 0 & 0 & ... & 0 & 0 & -1 \\ -1 & 1 & 0 & ... & ... & ... & 0 \\ 0 & -1 & 1 & ... & ... & ... & 0 \\ ... & ... & ... & ... & ... & 1 & 0 \\ 0 & 0 & 0 & ... & ... & -1 & 1 \end{pmatrix} \tag{18}$$

is a difference operator and

$$\Theta = \begin{pmatrix} \phi_0(s_0) & \phi_1(s_0) & ... & \phi_{N-1}(s_0) \\ \phi_0(s_1) & \phi_1(s_1) & ... & \phi_{N-1}(s_1) \\ ... & ... & ... & ... \\ \phi_0(s_{M-1}) & \phi_1(s_{M-1}) & ... & \phi_{N-1}(s_{M-1}) \end{pmatrix} \tag{19}$$

is $M \times N$ matrix depending on the location of the control points. The vector $\hat{A}$ that minimizes (17) is

$$\hat{A} = (\Theta^T\Theta + \alpha\theta^T\theta)^{-1}\Theta^T X. \tag{20}$$

The vector $\hat{B}$ is obtained as $\hat{A}$ by replacing X by Y in equation (20). From $\hat{A}$ and $\hat{B}$ the new evenly spaced control points are computed from

$$q_i = [\Phi(s_i)^T\hat{A}, \Phi(s_i)^T\hat{B}], \tag{21}$$

where $s_i = i/(L-1)$, $0 \leq i \leq L-1$ and L is the number of the new control points, which can be different from the original number of control points. These are used in the sequel of the segmentation process.

3.3 Contours linking

In this step all carotid and plaque contours must be linked to their corresponding neighbors. Therefore, a correspondence problem arises at this moment. The contours are described by a list of control points, whose dimension is user-specified. To make the correspondence between two sets of points they first must be matched.

Here, the matching is performed by using an *Iterative Closest Point* (ICP) [34] algorithm. The alignment procedure is based on the reasonable assumption that rapid position variations in the centroids of contiguous contours are not

expectable to occur. Each contour (carotid or plaque) is coupled with the corresponding contour in the previous image using the ICP algorithm. The pairing is based on the distance criterion, i.e., the closest points, after rotation and translation performed by the ICP on two consecutive contours (images) and belonging to the same object (carotid or plaque) are considered paired. This process is repeated for the whole sequence of contours (images).

The pairing process is difficult in the bifurcation because two contours of the internal and external carotids are merged into one single contour of the common carotid. For this singular case, a special procedure was developed. The first contour of the bifurcation is splited in two contours, creating an artificial line in its middle region (see fig. 7), where the splitting points correspond to the intersection points of the two contours from the previous image. Each one of the virtual contours in the bifurcation is then paired with the corresponding contour in the previous image, not inside the bifurcation. The linking proceeds then from this image until the end of the sequence.

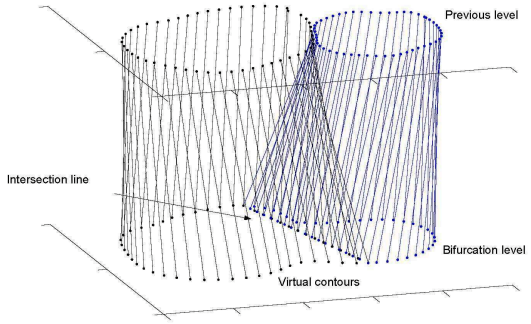

Figure 7. Bifurcation linking. The virtual contours (sets of points) created in the bifurcation level are linked to the correspondent control points in the previous plane.

3.4 Vertical alignment and smoothing

In order to compensate the small lateral displacements of the ultrasound probe during the acquisition process an alignment procedure of the contours is needed. The alignment is performed again in a pairwise basis, i.e., the global alignment is obtained by aligning all pairs of consecutive images.

The adjustment of two consecutive images is performed by minimizing an energy function involving translation vectors associated with each image. In order to obtain smooth surfaces, smooth variations of consecutive alignment vectors are required, which are achieved by introducing a regularization parameter. The energy function to be minimized, used to estimate the translation vectors is,

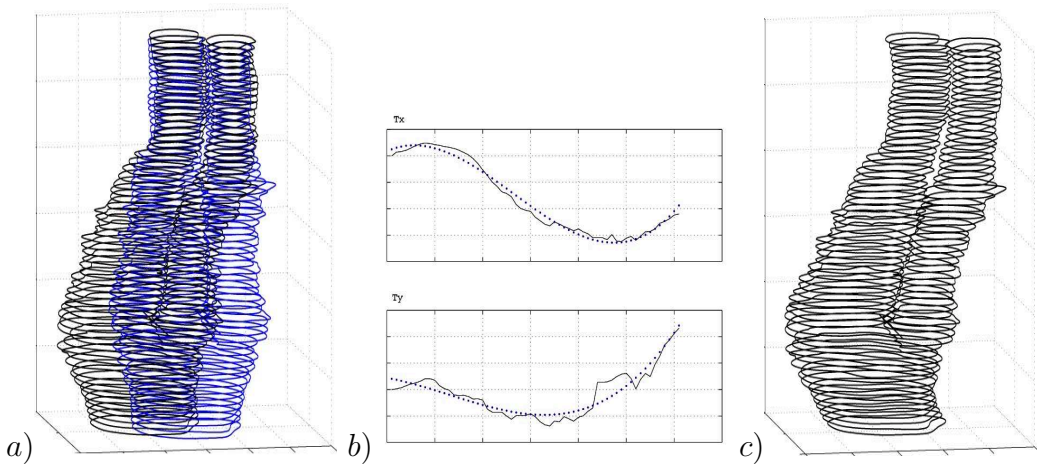

Figure 8. Vertical smoothing procedure. a) Absolut alignment (blue line) of the original contours (black line). b) Estimated translation vectors components in x and y (black line) directions and corresponding smoothed version (blue dots). c) Corrected alignment, using dynamic mean.

$$E_i = \sum_{k=0}^{L-1} [p_i(k) - p_{i-1}(k) - t_i]^2 + \alpha e_i^2, \tag{22}$$

where $p_i(k)$ is the k-th control point of the i-th contour, t_i is the misalignment compensation translation vector associated with the i-th image, $e_i = t_i - t_{i-1}$ are the differences between consecutive vectors, and α is the regularization parameter. Using matrix notation leads to

$$E_i = (P_i - P_{i-1} - \theta t_i)^T (P_i - P_{i-1} - \theta t_i) + \alpha (t_i - t_{i-1})^T (t_i - t_{i-1}), \tag{23}$$

where

$$P_i = [p_{ix}(0), p_{iy}(0), p_{ix}(1), p_{iy}(1), ..., p_{ix}(L-1), p_{iy}(L-1)]^T, \tag{24}$$

$$t_i = [t_{ix}, t_{iy}]^T \tag{25}$$

and

$$\theta = \begin{pmatrix} 1\ 0\ 1\ ...\ 0\ 1 \\ 0\ 1\ 0\ ...\ 1\ 0 \end{pmatrix}^T. \tag{26}$$

The vector that minimizes (23) is

$$t_i = (\theta^T\theta + \alpha I)^{-1}[\theta^T(P_i - P_{i-1}) + \alpha t_{i-1}]. \tag{27}$$

The alignment result is shown in fig. 8a, where the estimated translation vectors are added to the positions of the control points, for each plane. In fig. 8b, it is shown the smoothed curve, fitted to the estimated translation vector components. These smoothed curves are subtracted to the estimated translation vector components to avoid alignment compensation of slowly real anatomical deviations between planes, not originated during the acquisition process. Therefore a moving average filter is used to remove the low spatial frequencies of the translation vectors components, i.e.,

$$\tau_i = t_i - \bar{t}_i \tag{28}$$

where $\bar{t}_i = \frac{1}{2L+1}\sum_{k=-L}^{L} t_{i+k}$ and L is the half width of the moving average window. Fig. 8c displays the correct alignment of the contours with this mean compensation.

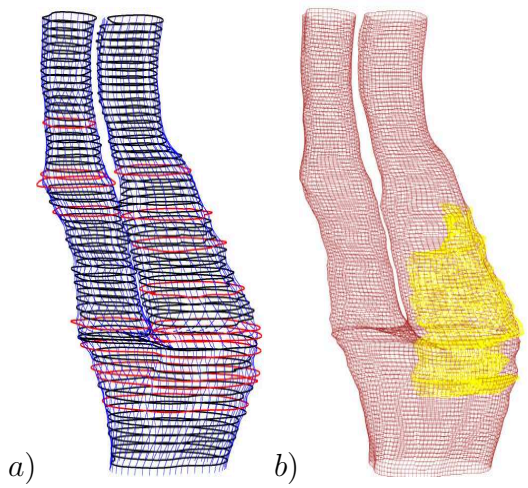

Figure 9. a) Linked control points, after application of the vertical alignment algorithm. b) 3D finite-element mesh representing the carotid artery and plaque.

After the alignment, a smoothing operation is applied to the vertical lines to attenuate discontinuities in the final mesh (see fig. 9a, where the primary deviations/ corrections are marked in red). This procedure is similar to the regularization performed in step 3.2.2.

3.5 VRML mesh generation

The final step of the reconstruction algorithm consists in the creation of a finite-element mesh (see fig. 9b), by applying different luminescence and transparency codes to the defined elements in order to facilitate the anatomy inspection. This information and criteria are used to create 3D virtual reality models of both carotid and atherosclerotic plaque, which are shown further ahead.

4 Plaque Characterization

In this section, methods for plaque characterization with respect to its vulnerability and instability are considered, based on textural features and morphology.

4.1 Background

A consensus on the morphology of atherosclerotic plaques indicates that characteristics of plaque echo-structure may play an important role in the early detection of unstable plaques, allowing a preventive treatment of atherosclerosis. Some early studies of carotid plaque morphology relied upon visual characterization based on subjective and qualitative analysis of ultrasonic B-mode images [35]. Currently, the study of carotid plaque morphology is made using computerized measurements, which provide an user-independent assessment of plaque echo-structure [36]. Plaque characterization is usually based on statistical analysis of the 2D ultrasound image [36,7], by using, for instance, a stratified grayscale median analysis and color mapping of the plaque [37], according to this parameter. The Gray-Scale Median (GSM) is one of the most important factors used on plaque diagnosis and it is generally used to classify plaques as echolucent ($GSM < 32$) or echogenic ($GSM > 32$). The total percentage of echolucent pixels (PEP), defined as the percentage of pixels with gray levels below 40, is also an important measure for characterization of plaque echogenicity. In fact, multiple regression analysis [36] have revealed that the GSM and the PEP are the variables more significantly related to the presence or absence of symptoms.

Recently, an activity index related to the plaque clinical risk [38,39] has been proposed. This index is the result of plaque classification according to several indicators, such as, plaque overall heterogeneity/homogeneity, surface disruption, degree of stenosis, global echogenicity and localization of the echolucent

region within the plaque.

It has been suggested that echogenicity, smooth surface and homogeneous texture indicate a stable plaque, while an irregular surface, echolucency, heterogeneous texture and the juxta-luminal location of the echolucent region are characteristics of potentially vulnerable plaques. A vulnerable plaque is also associated with thinning of the fibrous cap and infiltration of inflammatory cells that lead to surface ulceration and plaque rupture. Studies aiming at establishing a correlation between quantitative analysis based on ultrasound images and histological examination [40,41], have suggested that echolucent plaques have more lipid and hemorrhage, indicating inflammatory activity and therefore instability, while echogenic plaques are associated to the presence of more calcium and fibrous tissue, which are typically stable components within the plaque.

However, an accurate and reproducible assessment of morphological characteristics is limited when only cut planes of the plaque are considered, instead of its whole structure. There have been some recent published work, where 3D reconstructions of the entire plaque structure are considered. These studies aim to observe plaque ulceration [42] and to characterize plaque surface motion [43].

4.2 Ultrasonic Image Standardization

Image standardization is a crucial operation to allow the comparison of measures taken from different plaques, obtained with different ultrasound equipments, and different acquisition parameters (brightness/contrast).

Hence, the characterization is subject to significant interobserver variability and it is necessary to introduce image standardization methods, in order to garantee reproducibility and comparability of plaque characterization results. Most 2D studies of carotid plaque echo-structure consider an image standardization procedure consisting in an algebraic scaling of the whole image [36,38].

The normalization procedure takes a representative noisy cross section of the carotid artery with two distinct echo-anatomic regions. These correspond to blood and to the adventitia layer, and are used to manually measure the respective GSM. The histogram of the pixels inside the atheromatous plaque is then manipulated to put the blood pixels in the range of 0-5 and the ones of the adventitia in the range of 185-195 (see fig. 10). The gray values of all the other pixels are linearly rescaled according to these constraints.

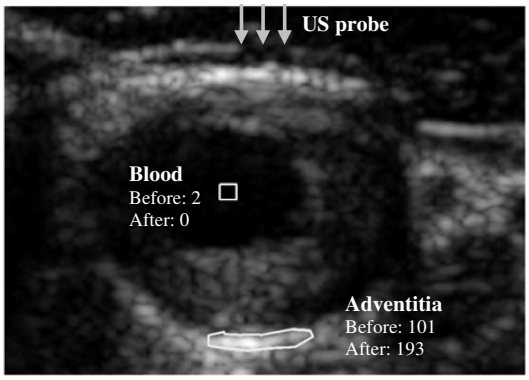

Figure 10. Standardization of a cross section of the carotid plaque. Blood and adventitia are outlined and its GSM values determined. The scale is adjusted ($GSM = 0$ for the blood and $GSM = 193$ for the adventitia).

4.3 Analysis of plaque ultrasonic features

In this sub-section it is described the application specifically developed to implement the 3D characterization of the plaque. The results obtained with this new approach are compared with the 2D based characterization methods, described in the literature. To perform the characterization using the classical methods, a longitudinal image of the atheromatous plaque is selected by an experimented medical doctor, which then analyze the plaque as follows (see fig. 11). The plaque contour is outlined manually and consensus measures, such as, GSM and PEP (percentage of pixels below 40) were determined using Adobe Photoshop (Adobe systems, Inc.). Furthermore, the degree of stenosis is calculated using a representative cross section and computing the ratio of carotid and lumen areas, combined with the hemodynamic assessment of the stenosis and calculation of the peak systolic and dyastolic velocities.

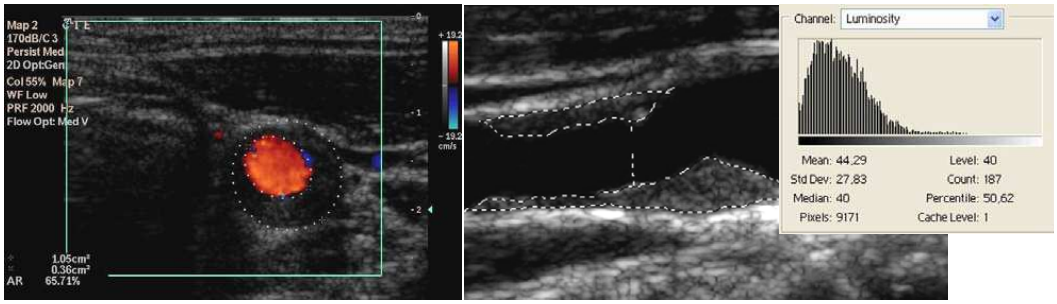

Figure 11. 2D analysis of carotid stenosis and plaque echoic features.

The alternative method, proposed in this work, is based on the automatic 3D characterization of the plaque, by using 3D ultrasound tools [42,43]. Plaque is globally and locally characterized considering the entire plaque structural information, as shown in fig. 12. Global measures, like plaque volume and extension, degree of stenosis and grayscale median (GSM) are computed. However, GSM analysis may not necessarily reflect the presence of particular unsta-

ble regions since it represents a median value of the whole plaque. Therefore, a local analysis is also performed by using space varying statistical parameters, such as mean, median, variance, standard deviation, skewness and curtosis. This method makes it possible to globally characterize heterogeneity and echogenicity of plaques, as well as identify possible active and unstable *foci* inside the plaque. Plaque echogenicity can be estimated using first-order

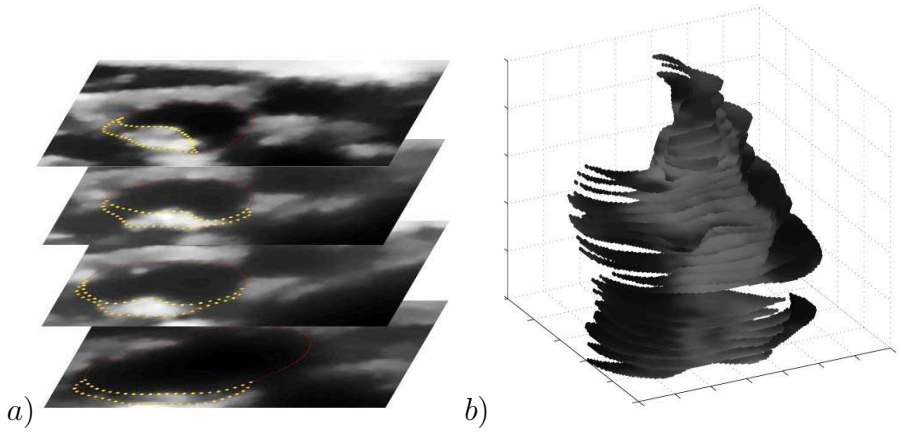

Figure 12. a) Automatic plaque segmentation. b) 3D ultrasound voxel-based reconstruction of the carotid plaque from the extracted contours.

statistics such as mean and median. By selecting regions inside the plaque where these statistics are below a given threshold (e.g. < 32 in $[0, 255]$ scale), it is possible to detect darker pixels, associated with unstable locations.

Other statistics, such as standard deviation, variance and curtosis are used to characterize heterogeneity, because they measure the dispersion of the pixel values distribution. By choosing high values, it is possible to identify regions with high pixel intensity variation and thus with high degree of heterogeneity.

In the scope of this work it was developed an application that allows the medical doctor to observe the carotid and atheromatous plaque, in a 3D environment and, simultaneously, select the threshold to be used in the detection of the regions of interest, in terms of echogenicity (intensity) and heterogeneity (texture), as shown in fig. 16. Inspection and automatic analysis of textural parameters, integrated in the 3D representation of the carotid anatomy is a new approach that improves the accuracy in the diagnosis of the atherosclerotic lesions.

5 Experimental Results

In this section, three examples of application of the new method for 3D diagnosis of atherosclerosis are shown, using one healthy and two diseased real

carotid arteries.

5.1 3D Reconstruction of Carotid Artery and Atherosclerotic Plaque

The overall 3D clinical analysis of the carotid atherosclerosis disease is performed in three steps: first, the carotid and plaque are segmented, by extracting its borders; secondly, the three-dimensional reconstruction is visualized on a virtual reality environment, and finally, the plaque is characterized. Three sequences of distinct carotid arteries are used, being one acquired from an healthy person (J.S.) and two from asymptomatic patients (F.C. and C.N.), obtained during their routine medical exams (ICVL, Lisbon).

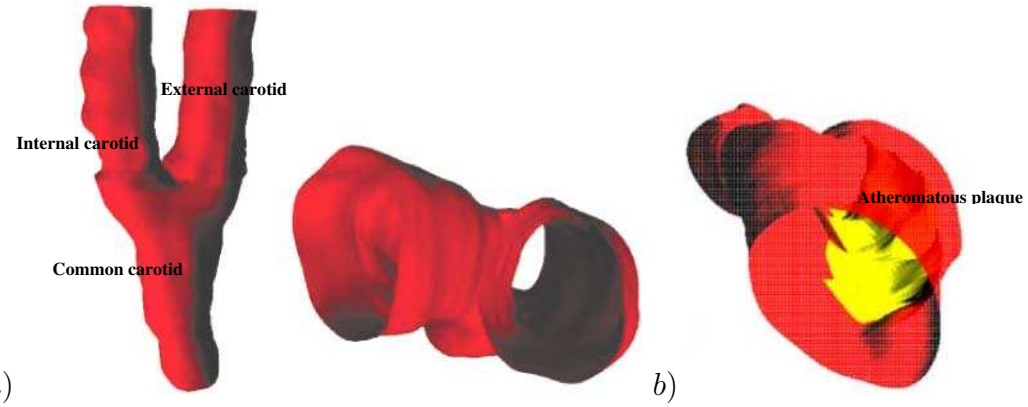

Figure 13. Three-dimensional representations of normal (a) and diseased (b) carotid arteries. Atherosclerotic plaque is shown in yellow.

The reconstruction results are displayed in a VRML environment where it is possible to manipulate and zooming the 3D models of the carotid and plaques to better inspect its anatomy. In this framework, it is easy and fast to evaluate the geometry and extension of the plaques and its precise localization inside the carotid. Fig. 13a shows the results from the reconstruction process for the normal carotid, where it is not detected an atheromatous plaque. On the contrary, fig. 13b shows the 3D reconstruction of the carotid and plaque, obtained from a patient (F.C.).

Taking a closer look on this diseased carotid (see fig. 14a) the luminal stenosis in the bifurcation region is clearly observed, which is due to the the presence of the atheromatous plaque. This 3D mesh was created by segmenting the carotid lumen and not the carotid wall which includes the plaque contribution (see fig. 14b). This first step in the plaque analysis is important in clinical terms, because it allows the evaluation of plaque extension and morphology.

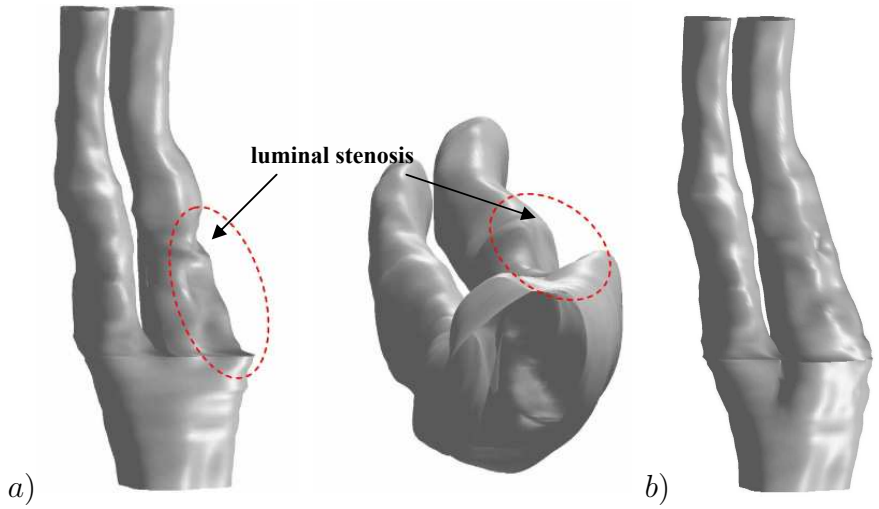

Figure 14. Diaseased carotid (FC) without (a) and after (b) considering plaque contribution. Luminal stenosis caused by the atheromatous plaque is indicated.

5.2 3D Plaque Characterization

The local assessment of plaque severity is also available at the diagnosis application, created in Matlab, for plaque characterization (see fig. 15). The results for plaque characterization are based on one clinical study of a diseased carotid (C.N.). Besides the carotid anatomy, the program also gives important global information, such as, plaque volume, maximum and mean stenosis, gray-scale median and PEP. In the clinical cases presented, the results are in overall concordance with the ones obtained by the conventional 2D approach: GSM of 37 (40, obtained by the conventional 2D examination), maximum stenosis of 61% (65%) and PEP, or percentage of echolucent pixels, of 53% (51%). The estimated plaque volume of $1,352mm^3$ is also important, but its relevance depends on the plaque extension. Even more important than the volume itself is the respective evolution along the time. This application is particularly suitable for this type of prospective clinical approach, allowing the comparison of the atherosclerotic plaque volume and extension at different stages of the disease.

The plaque echogenic analysis, in particular the GSM, determines whether (or not) the plaque is stable, considering the consensual threshold given in the literature ($GSM = 32$). This binary classification is however, most of the times, very simplist because it does not take into account if the GSM is closer to the threshold and, even worst, it does not give any information about the extension of the unstable regions inside the plaque.

Therefore, the local assessment of unstable regions within the plaque is needed

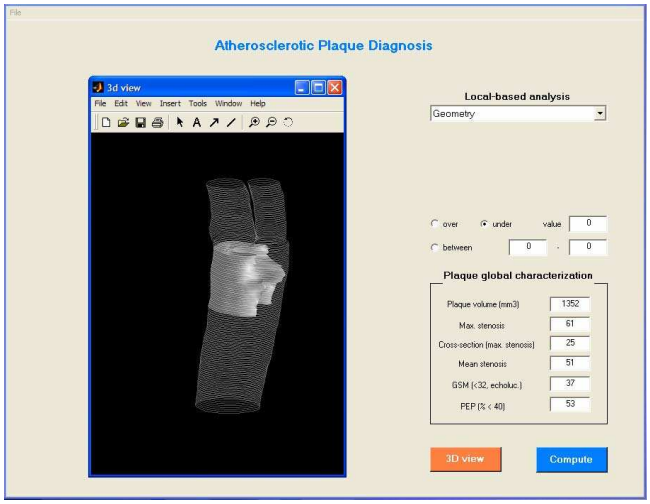

Figure 15. User-interface for plaque characterization written in-house (Matlab).

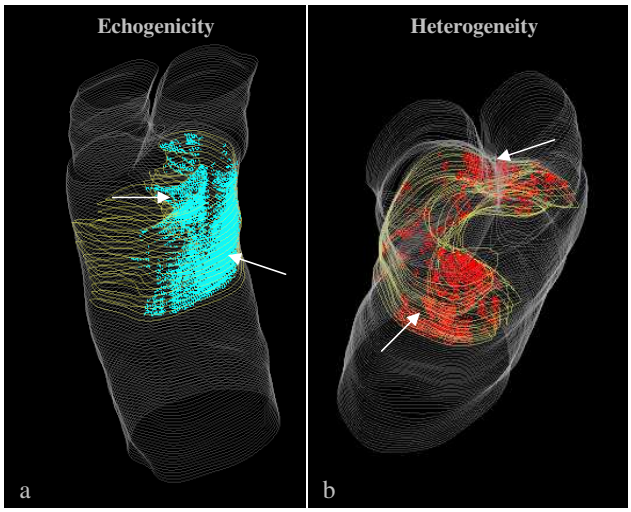

Figure 16. Local analysis, using median (a) and standard deviation (b). See text for explanation in detail.

to obtain information not provided by the global measurements. Fig. 16 shows the local analysis of the plaque using two different criteria to characterize the unstable regions: first, fig. 16a shows the most echolucent regions located at the central core of the plaque, where the median values are below 20, and fig. 16b shows the most heterogeneous regions, where the standard deviation is above 20 ($GSM \geq 20$), mainly in the peripheral locations of the plaque.

6 Conclusions

The importance of surgery for high degree stenosis, causing transient or minor ischemic strokes, has been well studied and documented. However, it remains

unclear which asymptomatic patients will benefit from carotid endarterectomy or other approaches, such as percutaneous transluminal angioplasty with stent placement. In this context, an increasing importance was given to plaque surface and ultrasonic morphological features, which are considered useful criteria for stratification of patients according to different stroke risk categories [44].

The goal of this project is to describe a computer-based tool for plaque characterization, involving the reconstruction of a three-dimensional mesh of the carotid artery and the plaque, and a volume-based tool for the assessment of the carotid plaque state. Hence, segmentation and extraction of the voxels from the 3D data set representing the carotid plaque makes it possible, not only to quantify the plaque volume, but also to globally compute its GSM and other textural parameters. This strategy may provide an important stage in the assessment of patients with asymptomatic carotid stenosis, making the clinical decision for surgical intervention easier.

The software that implements the reconstruction and plaque characterization algorithms allows a complete medical exam in a period of about one hour, including image acquisition. This good performance is achieved because the program is completely semi-automatic, which means the carotid and plaque are automatically segmented. Nevertheless, the medical doctor can interfere in the reconstruction process at anytime. Other important feature of this method is the spatial locator absence in the acquisition setup, meaning that only a common ultrasound equipment and a personal computer are required.

The first results obtained with this new method, in some clinical cases, agree with those obtained with the traditional 2D characterization method. However, a large set of clinical data is being acquired in order to allow a more accurate validation of the new method. The local assessment of the echogenicity and heterogeneity of the plaque is proposed in this work, allowing a clear improvement in the accuracy of the diagnosis, namely, when compared with the global measures. For instance, the most important parameter, GSM represents a median value of the whole atherosclerotic volume and therefore may not necessary reflect the presence of regional unstable (echolucent) regions.

Finally, this new approach, which is used to characterize the atherosclerotic lesions in the carotid, is implemented in an user-friendly application, allowing a fast and clear evaluation of the carotid and plaque anatomies and morphologies by the medical doctor.

References

[1] Zarins C.K., Xu C., and Glagov S. Atherosclerotic enlargement of the human abdominal aorta. *Elsevier Sc. Ireland*, pages 157–164, 2001.

[2] ACAS. Clinical advisory: carotid endarterectomy for patients with asymptomatic internal carotid artery stenosis. *Stroke*, 25(12):2523–2524, 1994.

[3] Executive Committe for the Asymptomatic Carotid Atherosclerosis Study. Endarterectomy for asymptomatic carotid stenosis. *J. Am. Med. Assoc.*, 8:273–1421, 1995.

[4] Landry A., Spence J.D., and Fenster A. Measurement of carotid plaque volume by 3-dimensional ultrasound. *Stroke*, 35:864–869, 2004.

[5] Stoitsis J., Golemati S., Nikita K.S., and Nicolaides A.N. Characterization of carotid atherosclerosis based on motion and texture features and clustering using fuzzy c-means. In *Proceedings of the 26th Annual International Conference of the IEEE EMBS*, September 1-5 2004.

[6] Barnett H.J.M., Meldrum H.E., and Eliasziw M. The appropriate use of carotid endarterectomy. *Can. Med. Assoc.*, 166:1169–1179, 2002.

[7] Pedro L.M., Pedro M.M., Goncalves I., Carneiro T.F., Balsinha C., Fernandes e Fernandes R., and Fernandes e Fernandes J. Computer-assisted carotid plaque analysis: characteristics of plaques associated with cerebrovascular symptoms and cerebral infarction. *Eur J Vasc Endovasc Surg*, 19:118–123, 2000.

[8] Loizou C.P., Pattichis C.S., Istepanian R.S.H., Pantziaris M., and Nicolaides A. Atherosclerotic carotid plaque segmentation. In *Proceedings of the 26th Annual International Conference of the IEEE EMBS*, September 1-5 2004.

[9] Mao F., Gill J., Downey D., and Fenster A. Segmentation of carotid artery in ultrasound images. In *Proceedings of the 22nd Annual EMBS international Conference*, July 23-28 2000.

[10] Liguori C., Paolillo A., and Pietrosanto A. An automatic measurement system for the evaluation of carotid intima-media thickness. *IEEE Trans. on Intsrumentation and Measurment*, 50(6), December 2001.

[11] Theocharakis P., Kalatzis I., Dimitropoulos N., , and Cavouras D. Computer based analysis of ultrasound images for assessing carotid artery plaque risk. In *Proceedings of the 3th International Symposium on Image and Signal Processing and Analysis*, 2003.

[12] Christodoulou C.I., Pattichis C.S., Pantziaris M., and Nicolaides A. Texture-based classification of atherosclerotic carotid plaques. *IEEE Transactions on Medical Imaging*, 22(7), 2003.

[13] Fenster A., Downey D.B., and Cardinal H.N. Three-dimensional ultrasound imaging. *Phys. Med. Biol.*, 46:6799, 2001.

[14] Carotid3d. http://users.isr.ist.utl.pt/ jseabra/software/carotid3D/.

[15] Abbot J. and Thurstone F. Acoustic speckle: Theory and experimental analysis. *Ultrasound Imaging*, 1:303–324, 1979.

[16] Dias J., Silva T., and Leitão J. Adaptive restoration of speckled SAR images using a compound random markov field. In *Procedings IEEE International Conference on Image Processing, Vol.II*, pages 79–83, Chicago, USA, October 1998. IEEE.

[17] Burckhardt C. Speckle in ultrasound b-mode scans. *IEEE Transations on Sonics and Ultrsonics*, SU-25(1):1–6, January 1978.

[18] Zeng Z. and Cumming I. Bayesian speckle noise reduction using the discrete wavelet transform. In *International geoscience and remote sensing symposium*, pages 6–10, July 1998.

[19] Prager R.W., Gee A.H., Treece G.M., and Berman L.H. Decompression and speckle detection for ultrasound images using the homodyned k-distribution. *Pattern Recogn. Lett.*, 24(4-5):705–713, 2003.

[20] Nascimento J., Sanches J.M., and Marques J.S. A method for the dynamic analysis of the heart using a lyapounov based denoising algorithm. In *Proceedings IEEE EMBC 2006*, New York City, USA, August 30-September 3 2006. IEEE International Conference of the Engineering in Medicine and Biology Society (EMBS).

[21] Sanches J. and Marques J.S. Image denoising using the lyapunov equation from non-uniform samples. In *Proceedings ICIAR 2006*, Póvoa de Varzim, , Portugal, September 2006. International Conference on Image Analysis and Recognition.

[22] Bartels R.H. and Stewart G.W. Solution of the matrix equation a x + xb =c. *Communications of the ACM*, 15(9):820–826, September 1972.

[23] Barraud A.Y. A numerical algorithm to solve a xa - x = q. *IEEE Transactions Automatic Control*, AC-22:883–885, 1977.

[24] Calvetti D. and Reichel L. Application of adi iterative methods to the restoration of noisy images. *Journal SIAM Matrix Anal. Appl.*, 17(1), 1996.

[25] Besag J.N. On the statistical analysis of dirty pictures. *J. R. Statist. Soc. B*, 48(3):259–302, 1986.

[26] Vogel C.R. and Oman M.E. Fast, robust total variation-based reconstruction of noisy, blurred images. 7(7):813–824, 1998.

[27] Bioucas-Dias J., Figueiredo J., and Oliveira J. Total variation image deconvolution: A majorization-minimization approach. *IEEE ICASSP*, 2006.

[28] Sanches J., Bioucas Dias J.M., and Marques J.S. Minimum total variation in 3d ultrasound reconstruction. *IEEE International Conference on Image Processing - ICIP 2005*, September 2005.

[29] Banham M.R. and Katsaggelos A.K. Digital image restoration. *IEEE Signal Processing Magazine*, 14(2), March 1997.

[30] Figueiredo M. and Leitao J. Simulated tearing: An algorithm for discontinuity preserving visual surface reconstruction. *Proc. IEEE Conf. Computer Vision and Pattern RecoveryCVPR93*, page 2833, 1993.

[31] Huang T. Yang. G. and Tang G. A fast two-dimensional median filtering algorithm. *IEEE Transactions Acoust. Speech Signal Processing*, 27(1):13–18, 1979.

[32] Sonka M. and Fitzpatrick J.M. Handbook of medical imaging. *Medical image processing and analysis, SPIE Press*, 2, 2000.

[33] Xu C. and Prince J.L. Snakes, shapes, and gradient vector flow. *IEEE Transactions on Image Processing*, 7(3), March 1998.

[34] Besl P. and McKay N. A method for registration of 3-d shapes. *Trans. PAMI*, 14(2), 1992.

[35] Geroulakos G., Domjan J., Nicolaides A., Stevens J., Labropoulos N., Ramaswami G., and Belcaro G. Ultrasonic carotid artery plaque structure and the risk of cerebral infarction on computed tomography. *J. Vasc. Surg.*, 20(2):263–266, 1994.

[36] Elatrozy T., Nicolaides A., Tegos T., and Griffin M. The objective characterization of ultrasonic carotid plaque features. *Eur J Vasc Endovasc Surg*, 16:223–230, 1998.

[37] Sztajzel R. et al. Stratified gray-scale median analysis and color mapping of the carotid plaque: Correlation with endarterectomy specimen histology of 28 patients. *Stroke*, 36:741–745, 2005.

[38] Pedro L.M. Uma janela para a aterosclerose. a ultrassonografia de alta definicão no estudo da parede arterial. *PhD Thesis*, 2003.

[39] Pedro M.M. Gonalves I. Dias N.V. Fernandes e Fernandes R. Carneiro T.F. Balsinha C. Pedro L.M., Fernandes e Fernandes J. Ultrasonographic risk score of carotid plaques. *European Journal of Vascular and Endovascular Surgery*, 24:492–498, December 2002.

[40] Jespersen S.K., Granholdt M.-L.M., Wilhjelm J.E., Wiebe B., Hansens L.K., and Sillesen H. Ultrasonic carotid artery plaque structure and the risk of cerebral infarction on computed tomography. *J. Vasc. Surg.*, 2:1065–1068, 1996.

[41] El-Barghouty N.M., Levine T., Ladva S., Flanagan A., and Nicolaides A. Histological verification of computerised carotid plaque characterisation. *Eur J Vasc Endovasc Surg.*, 11(4):414–416, 1996.

[42] Schminke U. MD, Motsch L., Hilker L., and Kessler C. MD. Three-dimensional ultrasound observation of carotid artery plaque ulceration. *Stroke*, 31(7):1651–1655, 2000.

[43] Meairs S. and Hennerici M. Four-dimensional ultrasonographic characterization of plaque surface motion in patients with symptomatic and asymptomatic carotid artery stenosis. *Stroke*, 30:1807–1813, 1999.

[44] Nicolaides A.N. Asymptomatic carotid stenosis and the risk of stroke. *Int Angiol.*, 14:21–23, 1995.